Numerical simulation with hardening soil model parameters of marine clay obtained from conventional tests

Samaila Saleh[1,2] · Nor Zurairahetty Mohd Yunus[1] · Kamarudin Ahmad[1] · Khairun Nissa Mat Said[1]

Abstract

Over the last decades, numerical modelling has gained practical importance in geotechnical engineering as a valuable tool for predicting geotechnical problems. An accurate prediction of ground deformation is achieved if models that account for the pre-failure behaviour of soil are used. In this paper, laboratory results of the consolidated drain (CD) triaxial compression tests and one-dimensional consolidation tests of marine clay were used to determine the hardening soil model (HSM) parameter for use in Plaxis 3D analyses. The parameters investigated for the HSM were stiffness, strength and advanced parameters. The stiffness parameters were secant stiffness in CD triaxial compression test (E_{50}^{ref}), tangent stiffness for primary oedometer loading test (E_{oed}^{ref}), unloading/reloading stiffness (E_{ur}^{ref}) and power for the stress-level dependency of stiffness (m). The strength parameters were effective cohesion (c'_{ref}), effective angle of internal friction (ϕ') and angle of dilatancy (ψ'). The advanced parameters were Poisson's ratio for unloading–reloading (v) and K_0-value for normal consolidation $\left(K_o^{nc}\right)$. Furthermore, Plaxis 3D was used to simulate the laboratory results to verify the effectiveness of this study. The results revealed that the stiffness parameters $E_{50}^{ref}, E_{oed}^{ref}, E_{ur}^{ref}$ and m are equal to 3.4 MPa, 3.6 MPa, 12 MPa and 0.7, respectively, and that the strength parameters c'_{ref}, ϕ', ψ' and K_o^{nc} are equal to 33 kPa, 17.51°, 1.6° and 0.7, respectively. A final comparison of the laboratory results with the numerical results revealed that they were in accordance, which proved the efficacy of the study.

Keywords Marine clay · Plaxis 3D · Hardening soil model · Model parameters

1 Introduction

The application of numerical analysis in geotechnical engineering is becoming a popular and common practise in enhancing engineering projects [1]. Nevertheless, the quality of any calculation rests on the suitability of the model assumed in the study. Generally, an accurate forecast of ground deformation can only be achieved when models that account for the pre-failure behaviour of soil are used [2, 3]. Modelling such behaviour with non-linear elasticity is characterised as a robust disparity in stiffness of soil, which is influenced by the degree of strain levels that occurs at stages of construction. Stiffness at pre-failure is crucial in modelling distinctive geotechnical problems such as retaining walls, supporting deep excavations or excavating a tunnel in a developed city.

Although linear constitutive models are commonly used in numerical analyses [4–8], actual soil behaviour is not as simple as it is represented in simple linear constitutive models. Soil behaviour is complicated in nature because soil is a multi-phase material that exhibits not only elastic, plastic and non-linear deformations but also irreversible plastic strains [9]. Depending on the stress history, soil may be compressed or dilated. Elasto-plastic models with linear elasticity such as the Mohr–Coulomb model (MCM) cannot reproduce a change in stiffness, as

✉ Samaila Saleh, samailasaleh@graduate.utm.my | [1]School of Civil Engineering, Universiti Teknologi Malaysia, Johor Bahru, Malaysia. [2]Department of Civil Engineering, Hassan Usman Katsina Polytechnic, Katsina 820241, Nigeria.

shown between points A, B and D in Fig. 1. Soil stiffness depends on the degree of stress-levels and deformations of soil are time-dependent. Indeed, soil behaviour is considered to be elastic in the small strain range; soil stiffness is nearly recoverable in unloading conditions. However, in the analysis of pre-failure non-linearities of soil behaviour, one may observe a substantial variation of stiffness starting from very small to very large shear strain.

Engineers who are looking for reliable forecasts of engineering system response and who apply linear-elastic, perfectly plastic models in the finite element analysis may underrate ground deformation. Numerical analyses in the MCM do not differentiate loading and unloading stiffness moduli, hence leading to an unrealistic lifting of the retaining wall linked with the unloading of the bottom of the excavation [10]. Similarly, Mohr–Coulomb assumed linear-elastic soil behaviour before failure; however, in reality, overconsolidated clays exhibit a reduction of stiffness at stress-levels below the typical expected values that cause failure [11]. Furthermore, the MCM assumes that stiffness parameters are not dependent on the stress-level. Therefore, it cannot symbolise a change in plastic strains, whilst unloading the soil.

The hardening soil model (HSM) is an advanced elasto-plastic constitutive model that is used for simulating both stiff and soft soil behaviours [12]. HSM also relates stiffness parameters to the stress-level and simulates the development of plastic strains under compressive loading. HSM is an extension of the hyperbolic model established by Duncan and Chang [13]. It supersedes the Duncan and Chang [13] model by using plasticity theory instead of elasticity

theory. It also includes the dilatancy of soil and introduces a yield cap. The yield surface of the HSM can expand as a result of plastic straining, unlike the elastic perfectly plastic model in which the yield surface is fixed in a principal stress space. At very low strain levels ($< 10^{-5}$) most soils exhibit higher stiffness than at engineering strain levels, and this stiffness varies non linearly with strain. In that case, the hardening soil model with small-strain (HSsmall model) is ideal for the analyses of both static and dynamic tasks [14]. HSsmall model is a modification of the HS model, which is concerned with improving soil stiffness in small strains.

HSM has two types of hardening: shear and compressive hardening. The difference between the two is that shear hardening is used for modelling permanent strains caused by principal deviator loading, whereas compression hardening is used for modelling permanent plastic strains caused by primary oedometric compression and isotropic load [15]. Despite the mathematical intricacy of the HSM, its parameters can be obtained from conventional soil tests due to their clear physical meaning. Therefore, in this paper, HSM parameters of marine clay (MC) were determined by using CD triaxial compression and oedometer test results. Furthermore, a simulation of the laboratory result was conducted in the Plaxis 3D software. The laboratory test results were validated with the numerical results to verify the effectiveness of this study.

Information from the literature revealed that some few studies have been performed on determination of model parameters. For example, Wu and Tung [16] developed a protocol for determining HSM parameters of gravelly soils using result of triaxial compression test. Their findings revealed the model parameters determined showed very good simulation of the measured data from triaxial tests and fields experiments with applied loads of up to 1000 kPa. Similarly, triaxial behaviour of riverbed and blasted quarried rockfill materials was modelled by Honkanadavar and Sharma [17] with HSM using triaxial compression results. Their results showed that the analysis of the elastic and shear strength parameters of the simulated and experimentally determined parameters found that both findings were closely matched. Finite element analysis and a parameter optimization algorithm were combined by Calvello and Finno [18] to effectively calibrate a soil model by minimising errors between experimental and numerical result. The obtained results indicated that the computed results match the experimental data. Stiffness parameters of residual soil at a deep excavation construction site in the Kenny Hill Formation were determined [19]. The result of parametric studies using HSM demonstrated that the horizontal deflection of the wall at each point of excavation was reasonably predictable with clear correlations between stiffness parameters and N value of standard penetration test. Application of the HS model has shown
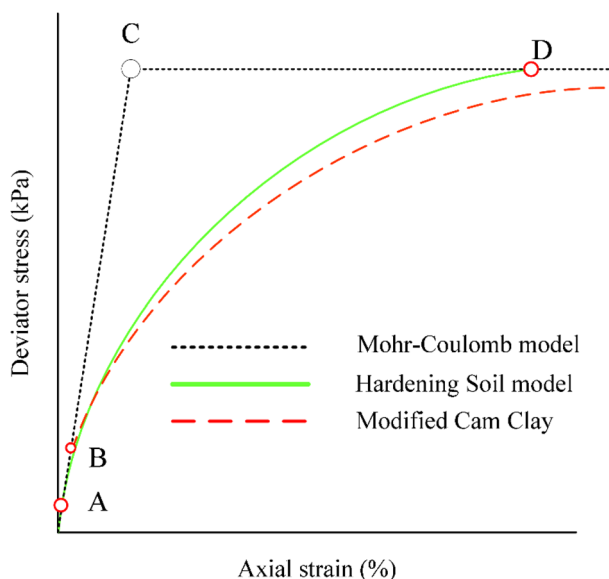

Fig. 1 Comparison of stress–strain curves of different models for drained triaxial compression

that the model is not only suitable for the study of the case of the Kenny Hill Formation, but can also be applied from a practical point of view to similar soils with these types of problems. The above and many more studies, such as those of [18, 20, 21] have led to research interest in determine HSM parameter of MC using results of CD triaxial compression test, oedometer test and particles size distribution test.

2 Material and method

The material used for this research is a disturbed sample of MC collected from Batu Pahat, Malaysia. The collected MC sample was air-dried, pulverised and stored in plastic containers. Index tests were conducted on the MC sample to identify and classify the soil. The results of the index tests were as previously reported [22], and MC was classified as clay of high plasticity (CH).

2.1 Consolidated drain (CD) triaxial compression test

The shear strength of the MC was measured using CD triaxial compression test following BS:1377-8 [23]. The cylindrical specimens (size of 38 mm diameter and 76 mm) were also prepared from remoulded MC mixed at the optimum moisture content [24]. To enhance the rate of saturation and consolidation, a vertical drain was fixed around the sample (see Fig. 2a) using filter paper, then placed in the triaxial cell, as shown in Fig. 2b. Important devices of the triaxial machine, such as the load cell, linear vertical displacement transducer (LVDT), volume change and pressure transducers, were calibrated prior to the beginning of the test. The equipment was connected to a computer's high-precision efficient real-time data acquisition function for automated recording and processing of data.

Using the method of back-pressure saturation, the saturation was achieved. Throughout the saturation stage, a 10 kPa backpressure difference was maintained until a Skempton B-check of at least 0.95 was obtained [25]. Subsequently, after completion of the saturation of the specimen, the next stage was consolidation with varying effective stresses of 100 kPa, 200 kPa and 300 kPa [26]. Shearing was carried out at the end of the consolidation stage by estimating the shearing rate from t_{100} of the consolidation curve using Eq. (1). During the shearing, the drainage line was opened (back pressure valve). The triaxial test equipment used in this research is shown in Fig. 2c.

$$t_f = 14 \times t_{100} \qquad (1)$$

t_f, time to failure for CD test with side drain; t_{100} is the intercept of tangent lines touching initial portion and horizontal portion of volume change vs square root time curve of consolidation stage.

2.2 One-dimensional consolidation test

Test of MC consolidation characteristics was carried out as per of BS:1377-5 [27] using unsaturated MC. The specimen was prepared for soil compacted in cylindrical moulds with a diameter of 50 mm and a height of 20 mm. The test was carried out using a load sequence ranging from 10 to 1000 kPa with twice the load increment ratio. The pressure was maintained constant for 24 h during each loading cycle. The unloading was carried out in a similar way at the end of the last loading cycle. The compression gauge readings and the corresponding time intervals were automatically recorded at every stage of the test using a data logger connected to the computer.

2.3 Particle size distribution

Due to the higher precision, reliability of results and speed of the operation, the particle size distribution of the MC was carried out using the Laser diffraction method following the standard ISO:13320 (2009) procedure [28, 29]. Approximately, 50 g of the air-dried MC sample was soaked for 24 h in a dispersion agent to come up with a solution. One litre of distiled water, 7 g of sodium carbonate and 33 g of sodium hexametaphosphate were used to produce the dispersion agent. The soaked MC was mixed for 30 min using a mechanical mixer to obtain a homogeneous solution for particle size distribution test using a Laser diffraction machine model LA960V2 HORIBA.

2.4 Numerical simulation of the laboratory results

The numerical simulation of the MC laboratory result was performed in a separate window in the Plaxis software. As shown in Fig. 3a, an input parameter was entered and the test was run. The deviator stress vs axial strain curve was selected (Fig. 3b), and the data were imported to excel where the curves of both numerical and experimental results were plotted.

3 Results and discussions

The following sub-section provides the discussion of both the experimental and numerical results.

3.1 Strength parameters

The strength parameters were obtained using the results of the CD triaxial compression test. The parameters

Fig. 2 Triaxial apparatus set up for the CD triaxial tests: **a** shows triaxial cell, **b** shows vertical drain in the triaxial sample and **c** complete triaxial machine


(a)

(b)

(c)
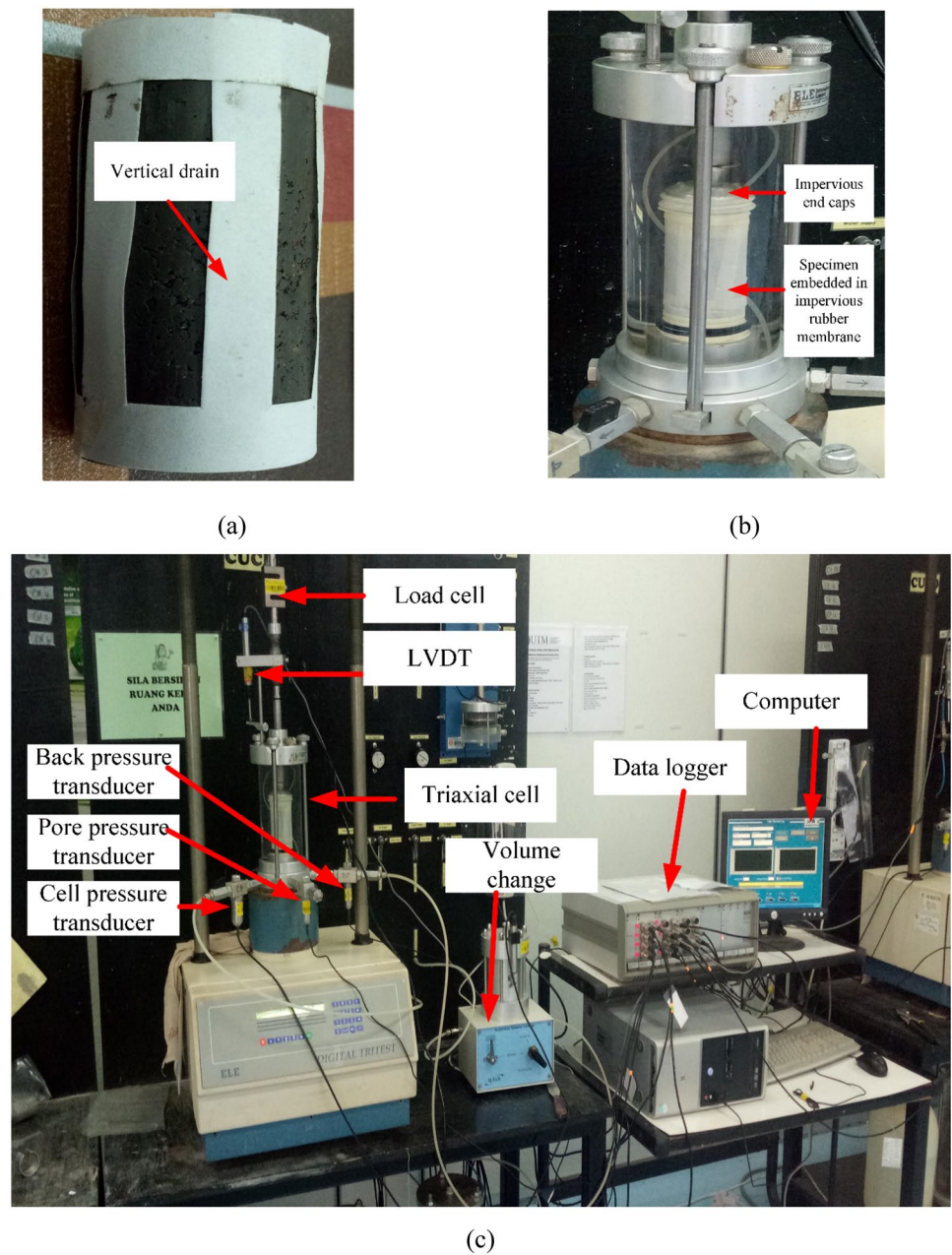
obtained were c'_{ref} (kN/m²), ϕ' (degree), and ψ' (degree). Three confining pressures were adopted in CD triaxial compression tests: 100 kPa, 200 kPa and 300 kPa, respectively. The summary of the effective major and minor principal stresses at the failure of the three specimens are presented in Table 1. Figure 4 shows the Mohr circles of effective stresses, which specifies the conditions at the failure of the CD triaxial compression test. From the results, the strength parameters, c'_{ref} and ϕ' were found to be 33.58 kPa and 17.51°, respectively.

The dilatancy angle, ψ' was obtained from the gradient of the axial strain-volumetric strain curve, as shown in

Fig. 5. Based on the curve, only 100 kPa confining pressure showed some or little dilatancy. When the confining pressure exceeds 100 kPa, the dilatancy disappears [30, 31]. From Fig. 5, for the 100 kPa confining pressure curve, using 0.0564 as the value for d, the dilatancy angle computed using Eq. (2) was 1.6 degrees.

$$\psi = -\sin^{-1}\left(\frac{d}{2-d}\right) \tag{2}$$
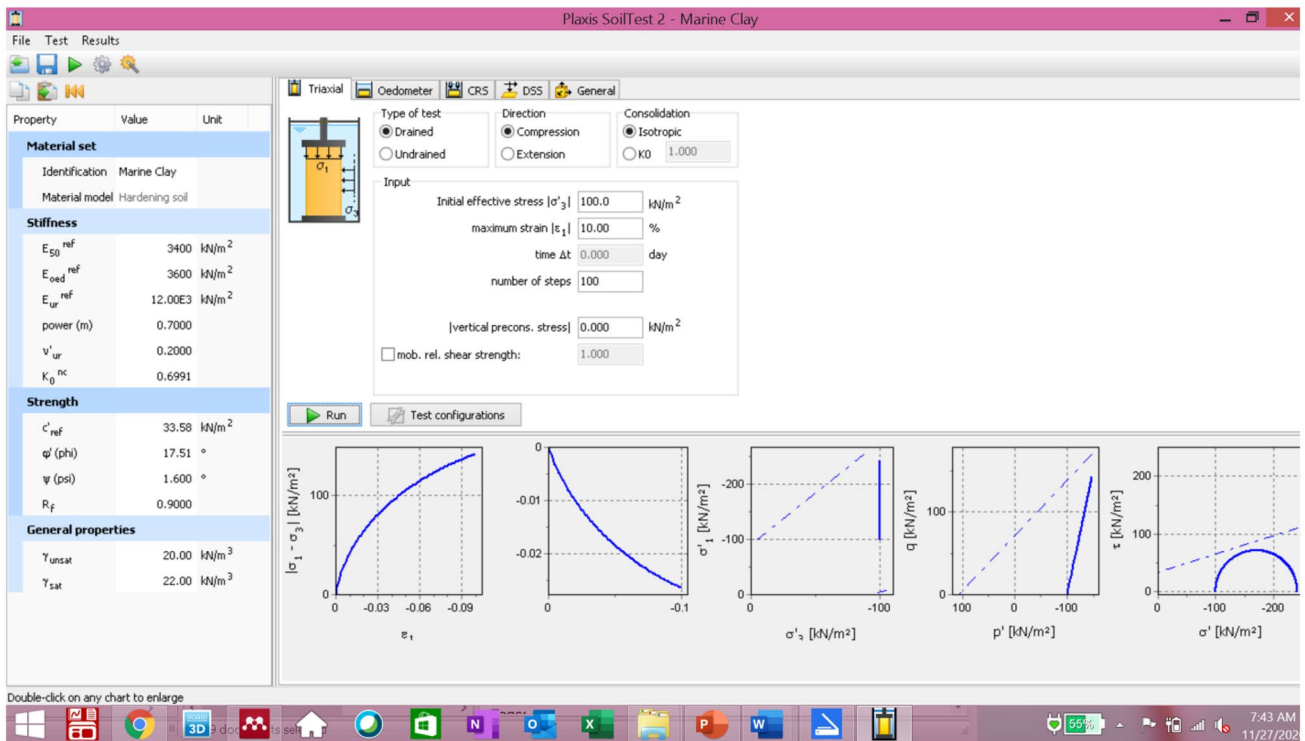
(a)
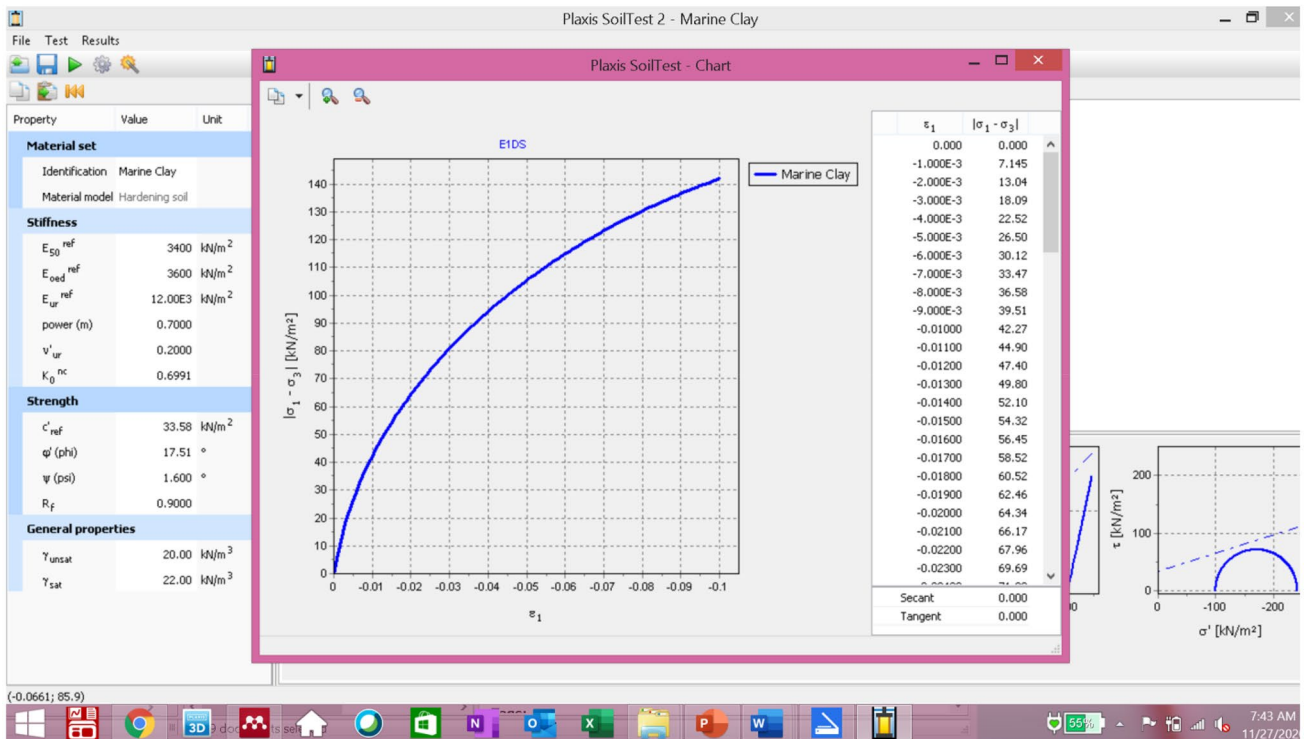
(b)

Fig. 3 Simulation of marine clay properties in Plaxis 3D **a** inputting the model parameters and **b** collecting the simulated results

Table 1 Summary of specimen details at failure during CD triaxial compression test

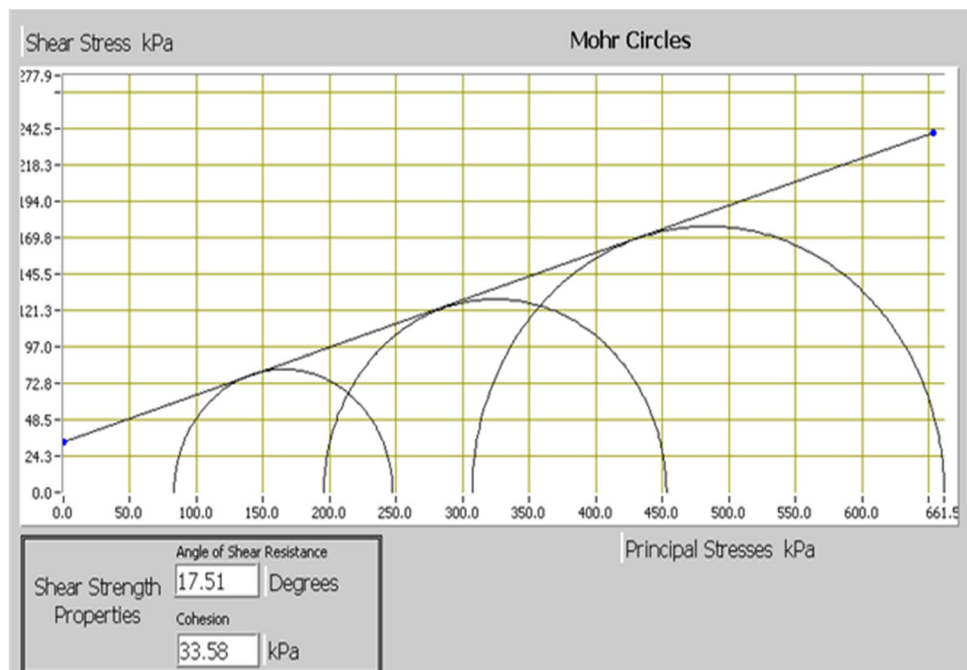| Specimen reference	Effective minor principal stress (σ_3') (kPa)	Effective major principal stress (σ_1') (kPa)
A	83.2	247.3
B	195.7	452.9
C	307.1	661.5

3.2 Stiffness parameter

The stiffness parameters were obtained using the results of the CD triaxial compression test and oedometer test. The parameters obtained were E_{50}^{ref} (kN/m^2) in the CD triaxial compression test, E_{oed}^{ref} (kN/m^2) for primary oedometer loading test, E_{ur}^{ref} (kN/m^2), and power for the stress-level dependency of stiffness, m.

The values for E_{50}^{ref} and m that were obtained by plotting the deviator stresses against the axial strains for each confining pressures are shown in Fig. 6. In addition, the moduli E_{50}, corresponding to each of them, were determined as 3159 kPa, 4296 kPa and 5428 kPa, respectively.

The value for stiffness stress dependency parameter m was obtained using the trend line based on Eq. 3. The values for the y variables were assigned as $\ln E_{50}$ and x variables as $\ln \left(\frac{\sigma_3' + c' \cot \phi'}{100 + c' \cot \phi'} \right)$ [32], as shown in Fig. 7. The slope of the trend line was the value for the stiffness stress dependency parameter m and was found to be equal to 0.7.

$$y = ax + b \tag{3}$$

The secant stiffness of the CD triaxial compression test (E_{50}^{ref}) was computed using Eq. (4) for each of the three respective effective stress, σ_3', using the corresponding moduli E_{50}, as shown in Table 2. The values for effective c', ϕ' and m were already obtained as 33.51 kPa, 17.58 0 and 0.7,
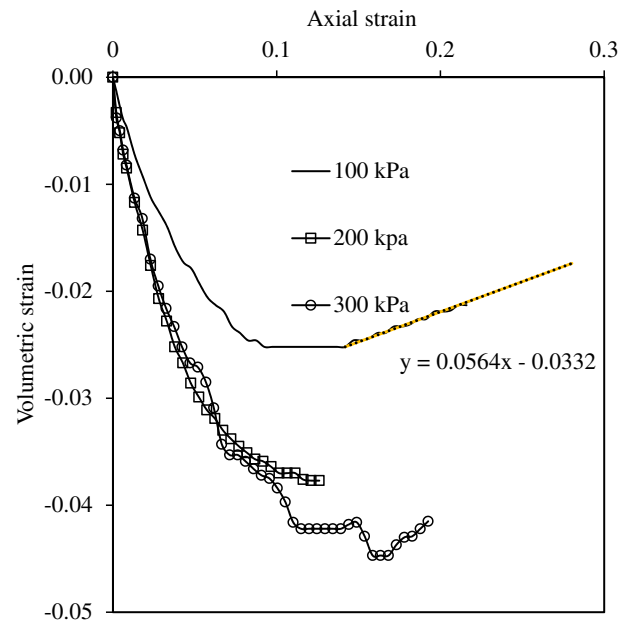
Fig. 5 Determination of dilatancy angle

Fig. 4 Mohr circle of CD triaxial compression test result
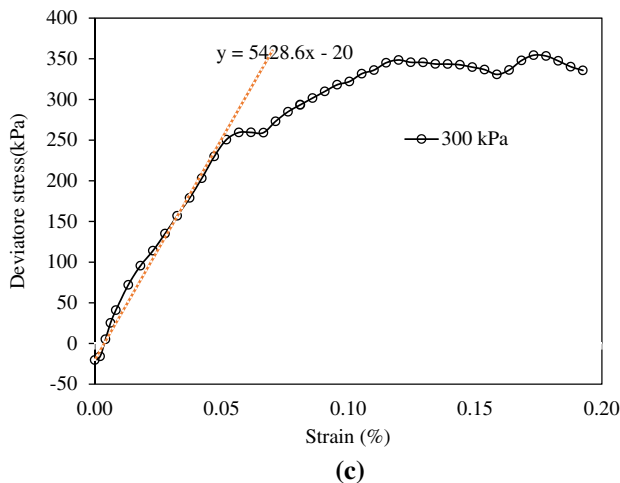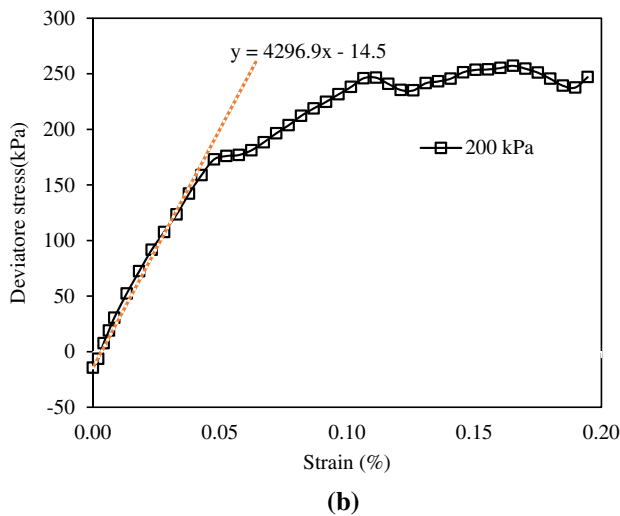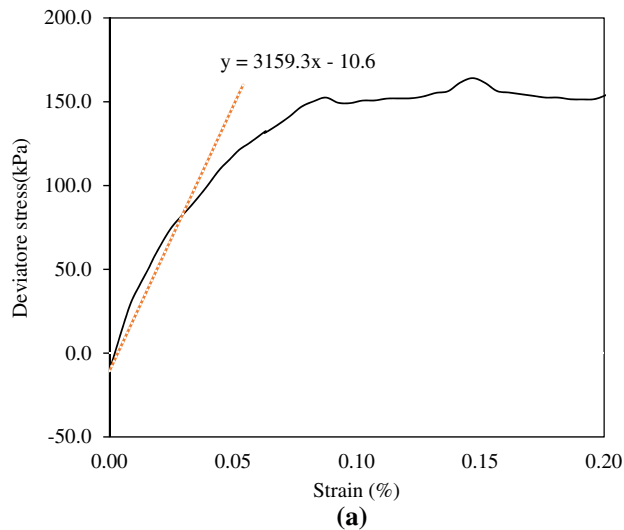
(a)

(b)

(c)

Fig. 6 Determination of E_{50} moduli from the curves of deviator stress vs axial strain of drained triaxial compression tests at **a** 100 kPa, **b** 200 kPa and **c** 300 kPa cell pressure
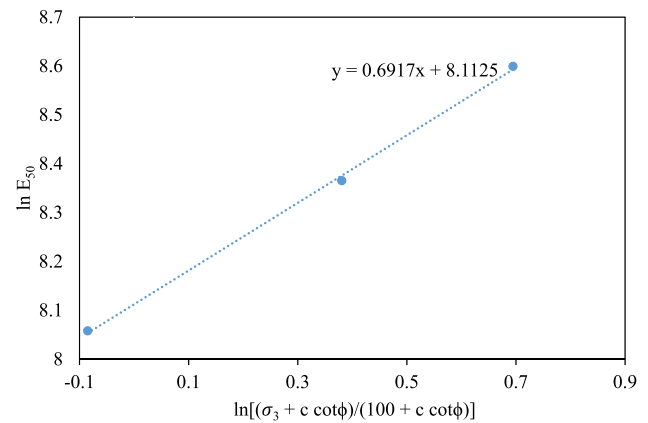

Fig. 7 Determination of stiffness stress dependency (m) parameter

respectively. Therefore, the average value of E_{50}^{ref} was found to be approximately 3.4 MPa.

$$E_{50} = E_{50}^{ref}\left(\frac{\sigma_3' + c'\cot\phi'}{100 + c'\cot\phi'}\right)^m \tag{4}$$

E_{50}^{ref}, secant stiffness in CD triaxial compression test (kN/m^2); E_{50}, moduli E_{50} corresponding to effective stress, σ_3' (kN/m^2); σ_3', effective minor principal stress (kN/m^2); m, power for stress-level dependency of stiffness (parameter m); c' (kN/m^2), effective cohesion; ϕ', effective angle of internal friction (degree); ψ', angle of dilatancy (degree).

The result of the consolidation test of MC is presented in Fig. 8. From the result, the compression index c_c was found to be equal to 0.1943. The tangent modulus E_{oed} and Oedometer tangent stiffness and E_{oed}^{ref} post-yielding of the primary loading was computed using Eqs. 5 and 6. The value of the E_{oed}^{ref} was computed to be equal to 3.6 MPa.

$$E_{oed} = \frac{2.3\left(1 + e^{ref}\right)\sigma_{oed}^{ref}}{c_c} \tag{5}$$

$$E_{oed} = E_{oed}^{ref}\left(\frac{\sigma_3' + c'\cot\phi'}{100 + c'\cot\phi'}\right)^m \tag{6}$$

Table 2 Determination of secant stiffness of the CD triaxial test, E_{50}^{ref}

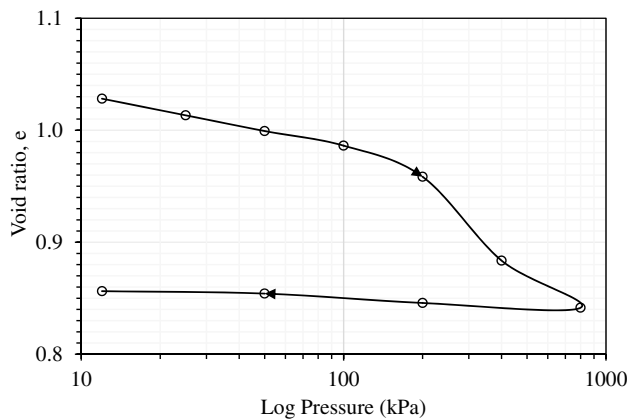| σ_3' (kPa)	E_{50} (kPa)	$\left(\frac{\sigma_3'+c'\cot\phi'}{100+c'\cot\phi'}\right)^m$	E_{50}^{ref} (kPa)
83.2	3159	0.94	3471.429
195.7	4296	1.31	3279.389
307.1	5428	1.62	3350.617
Average			3367.145

Fig. 8 Determination of Oedometer tangent modulus E_{oed} from the result of consolidation test

E_{oed}, oedometer tangent modulus; E_{oed}^{ref}, oedometer tangent stiffness; σ_{oed}^{ref}, stress at which the marine clay undergoes plastic straining; e^{ref}, Void ratio corresponding to stress σ_{oed}^{ref} at which the material undergoes plastic straining; c_c, compression index.

Note that σ_{oed}^{ref} and e^{ref} are relevant to the material that undergoes plastic straining, that is, the stress point that lies on the primary loading curve. The unloading–reloading modulus E_{ur}^{ref} was estimated to have a value varying between 3 and 5 times the E_{50}^{ref} Plaxis-3D [33] and Wang et al. [34].

3.3 Stiffness advanced parameters

The advanced stiffness parameters were estimated based on the recommendation of Plaxis-3D [33]. The parameters for the advanced stiffness were Poisson's ratio for unloading–reloading (default $v = 0.2$), reference stress for stiffnesses (default $p^{ref} = 100$ kN/m^2) and K_0-value for normal consolidation (default $K_o^{nc} = 1 - \sin \phi$). The recommended values for the stiffness advanced parameters are the default values [33].

3.4 Particle sizes distribution

The result of the particle size distribution of MC is shown in Fig. 9. From the result, particles smaller than 2 µm, particles between 2 µm and 50 µm and particles bigger than 50 µm were 3%, 75% and 22%, respectively. The result for the particle size distribution was also applied in the Plaxis software, whilst performing the simulation.

3.5 Comparison of experimental and numerical results

Table 3 shows a summary of the HSM parameters obtained for all the studies. The listed parameters were inputted into the HSM in Plaxis 3D software, and stress–strain curves from the CD triaxial compression tests were obtained. Figure 10 shows the comparison of the numerical and experimental results of the CD triaxial compression test of the MC at three different confining pressures. The comparison demonstrates that the HSM can simulate the stress and strain behaviour of the MC. The above comparison is also in agreement with the comparison report by Wang et al. [34].

3.6 Discussion of experimental results

Discussion of the properties of MC was carried out by comparing the properties of MC in this research with other MC properties from different parts of the world published

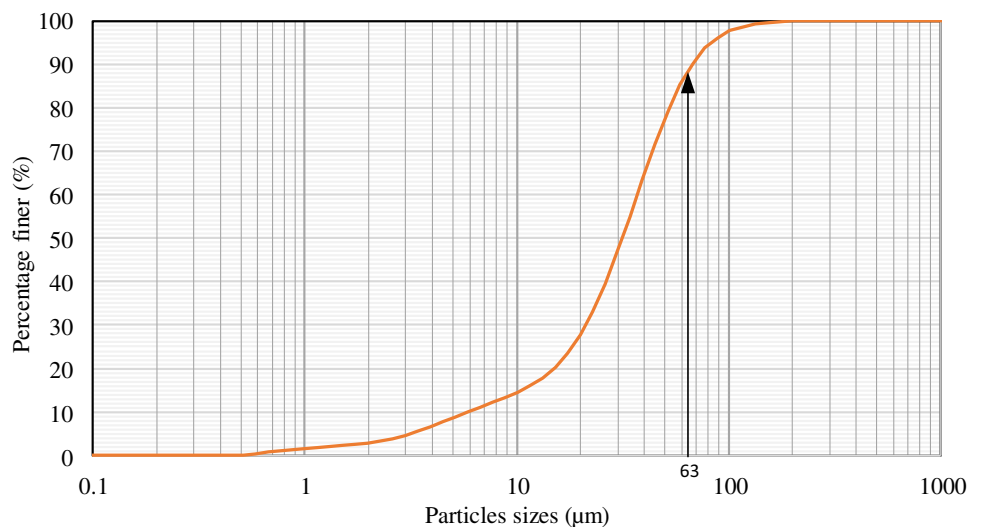**Fig. 9** Result for the particles sizes distribution

Table 3 Summary of experimental results

| Parameters	Unit	Values
Secant stiffness in CD triaxial compression test (E_{50}^{ref})	kN/m^2	3400
Tangent stiffness for primary oedometer loading test (E_{oed}^{ref})	kN/m^2	3600
Unloading/reloading stiffness (E_{ur}^{ref}))	kN/m^2	12,000
Stress-level of stiffness, m	–	0.7
Effective cohion, c' (kPa)	kN/m^2	33.58
Effective friction angle, ϕ'	degree	17.51
Dilatancy angle, ψ'	degree	1.6
Poisson's ratio, ν	–	0.2
Reference stress for stiffnesses p^{ref}	kN/m^2	100
K$_0$-value for normal consolidation, K^{nc}	–	0.7
Compression index, C_c	–	0.1943
Initial void ratio	–	1.0282
Saturated unit weight γ_{sat}	kN/m^3	22
Particles sizes ≤ 2 μm	%	3
Particles sizes 2–50 μm	%	75
Particles sizes ≥ 50 μm	%	22
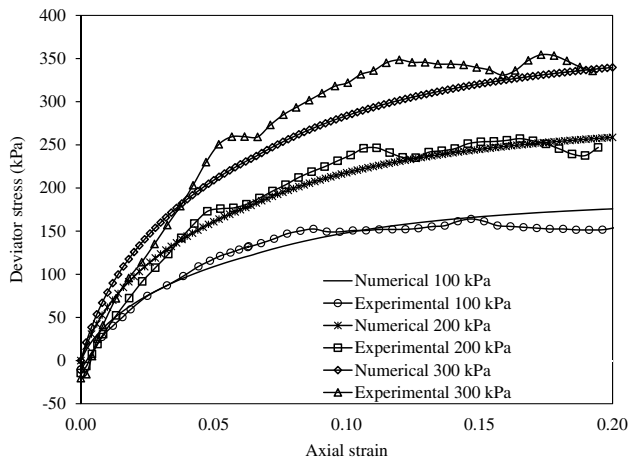
Fig. 10 Comparison of laboratory test with the numerical analysis

in the literature. The discussion covered in this paper is limited to the result of shear strength and consolidation properties of the MC as well as result of particles size distribution and numerical simulation of the HSM of the MC. Index properties, geochemistry, microstructure and toxicity of the MC are not cover in this paper because they were reported earlier in previous research [22, 35–37].

The shear strength of soil depends on the water content, mineral content and the degree of consolidation of the soil [38, 39]. Triaxial tests are commonly used to test the shear strength of the MC. In this research, the shear strength parameters of the MC were determined using consolidated drained (CD) triaxial tests. The result obtained showed that the effective cohesion, c' and effective angle of internal friction, ϕ' were found to be 33.58 kPa and 17.51°, respectively.

The c' values for the MC in this study is marginally higher than those reported for MC from central Iran and Kedda Malaysia [40, 41] whose both reported c' of 25 kPa. Likewise, another MC from south China sea [42], and Thaniland [43] had c' of 20 and 18 kPa, respectively. Similarly, Pakir [44] and Sunny and Joy [45] also recorded much lower value of c', 10 kPa and 9 kPa for MC collected from Johor Malaysia and Kerala India. On the other hand, the values of ϕ' for the MC in this research is lower than that MC from Thailand and Johor Malaysia in which ϕ' was equal to 25° and 22°, respectively [43, 44]. The value of the ϕ' was higher than that reported by Ouhadi et al. [40] who reported ϕ' of 15°.

Compression index (c_c), swelling index (c_s) and initial void ratio (e_o) are amongst the parameters that can be obtained from the consolidation test. The results of this research showed that the value for the c_c of MC are 0.194. Comparison of the consolidation properties of the MC in this research and other MC from published literatures showed that the c_c of the MC is about similar to the MC from Ningbo city, China [46] and Johor Malaysia [44] in which the c_c values were 0.18 and 0.22, respectively. The value of the c_c is lower than the other MC from Singapore [47, 48] in which the value ranges between 0.6 and 1.5. Other MC from Kedah Malaysia and Pathumthani Thailand were also reported to have relatively higher c_c value between 0.57 and 1.67 [41, 49].

The value c_s of the MC was 0.014, is slightly lower than that of MC from Perak Malaysia, Ningbo city China and Johor Malaysia in which their c_s values were 0.02, 0.035, and 0.04, respectively [44, 46, 50]. Singapore MC had c_s

Table 4 Comparison of the experimental values with the existing literature

Reference	Model type	Soil type	C_u (kPa)	ϕ (°)	ψ (°)	E_o (MPa)	V	E_{50} (MPa)	E_{eod} (MPa)	E_{ur} (MPa)	G_o (MPa)	K_o	γ^* (kN/m³)	C_c C_r	e_o	m
Ouahab et al. [58]	M-C	Clay	20	0		1000	0.49									
Abu El-Soud and Belal [59]	M-C	Sand	15	30	0	25,000	0.30									
Abbas et al. [6]	M-C	sand	1	37	5	19,000	0.30									
Naseer et al. [8]	M-C	Clay and Sand	54	–	–	4610	0.40						14.40			
			34	–	–	2532 1351	0.42						13.06			
			14-	–	–	25,000	0.44						12.72			
				30	1		0.30						15.50			
Zukri [60]	HSM	Kaoline	8	25	0	2420	0.30							0.256 0.058		
Skels and Bondars [61]	HSSM		54.03	31.35	0	–	–	13.6	13.6	40.8	120	2.17	23.4			
Wang et al. [34]	HSM	Sand	8.6	35.60	5.6	–	0.20	17.5	17.5	70	–	–	17.9	– –	0.28	0.5
Zukri et al. [62]	HSM	Kaoline	7	25	0	2420	0.30							0.256 0.058	2.39	0.336
Samadhiya [63]	HSM	Clay	5	25	0	–	–	2	2	10			17			1
	HSM	Granular pile	1	40	10			70	70	210			21			0.3
Momeni et al. [64]	HSM	Silty clay	10.41	12		4000	0.20	12.06	6.031	36.19		0.79	21.2			1
		Sand	0.08	29		21,552	0.20	25.86	25.86	77.6			19.5			0.5
		Sand	0.06	30.50		14,392	0.20	15.99	15.99	46.97			19.63			0.5
Zheng [65]	HSM	Clay	30	24				50	50	150						
	HSSM	Clay	30	24				50	50	150	200					
	HSM	Sand	1	35				50	50	150						
	HSSM	Sand	1	35				50	50	150	200					
Jamsawang et al. [43]	HSM	Clay	18	25			0.2	50	50	150			20			
Current paper	HSM	Marine clay	33.58	17.51	1.6	–	0.20	3.4	3.6	12	–	0.70	22	0.1943	1.0282	0.7

between 0.06 and 0.16 [47, 48]; similarly, Thailand MC has c_s values of 0.14 [49]. The value of e_o of the MC under review was 1.03, and it was slightly higher than the MC from Johor which has e_o equal to 0.85. The e_o value is slightly lower than the MC from Ningbo City China and Port Harcourt Nigeria which have e_o value 1.22 and 0.83 to 1.5, respectively [46, 51]. Other MC from Thailand, Perak Malaysia, Changi Singapore and South China Sea had higher e_o values that ranges between 1.8 and 3.3 [42, 47, 49, 50]. The variation in the consolidation properties of the various MC is linked to the water content, permeability, structural arrangement and porosity of the soil particles [52].

The results for the particle size distribution revealed that the proportion of fine particles below 63 μm (clay and silt) in the MC is about 88%. Ouhadi et al. [40] and Otoko and Simon [51] reported that MC from cental Iran and Port Harcourt Nigeria had 78% and 91% fine particles. Similarly, other MC from China and Thailand had proportion of fine particles between 94% and 96% [49, 53, 54]. Pakbaz and Alipour [55] and Sunny and Joy [45] both reported 97% as the proportion of fine particles in the MC from port of Imam Khomeini in southwest of Iran and Thopumpady, Ernakulam, Kerala India. The high composition of fine particles and the presence of swelling mineral like monmorillonite and illite in the MC are some of the reason that make MC problematic soil for construction purpose [56, 57].

3.7 Comparison of the model parameter with existing research

Table 4 presents a comparison of the HSM parameters with some other models' parameters reported in current studies. Generally, the majority of the models' parameters reported showed that the researchers used MCM. The model of shear strength parameters shows that cohesion ranges between 1 kPa and 54 kPa. Granular soil, sand and very soft clay are reported to have a lower value of cohesion.

The friction angle ranges between 0 and 40 degrees. Clay tested under undrained conditions has zero friction angle, whilst sand and granular soils have a higher friction angle. The result also shows that clay soils have zero dilatancies, whilst sand has a dilatancy angle that ranges between 1 and 10 degrees. By comparing the result of this paper and that of previous studies, it can be said that the values of the shear strength parameters fall within the range of the results reported by many researchers. Similarly, considering the result of stiffness parameters, the values for E_{50} and E_{oed} range between 2 and 50 MPa. Values for E_{ur} range between 10 and 150 MPa. Similarly, values

for parameter m range below 0.5 for sand and between 0.5 and 1 for clay soil. The said stiffness parameter for the current paper also falls within the range reported in prior research.

4 Conclusion

From the results obtained by CD triaxial compression test and one-dimensional consolidation tests, the shear strength and stiffness parameters of HSM of MC were determined. The findings could provide a useful reference for conducting numerical analyses on similar soil. The key results are as follows:

1. The values of shear strength parameters obtained are c'_{ref}, ϕ' and ψ', which are equal to 33.58 kPa, 17.51° and 1.6°, respectively. The stiffness parameters obtained are E_{50}^{ref}, E_{oed}^{ref}, E_{ur}^{ref} and m, which are equal to 3.4 MPa, 3.6 MPa, 12 MPa and 0.7, respectively.
2. A simulation of the laboratory result was conducted in the Plaxis 3D software. Comparison of curves for deviator stress versus the axial strain of the laboratory test results were and numerical results showed good fit and that verify the effectiveness of this study.

Compliance with ethical standards

References

1. Ikeagwuani CC, Nwonu DC (2019) Engineering emerging trends in expansive soil stabilisation: a review. J Rock Mech Geotech Eng 11(2):423–440. https://doi.org/10.1016/j.jrmge.2018.08.013

2. Phoon K, Tang C, Phoon K (2019) Characterisation of geotechnical model uncertainty. Georisk Assess Manag Risk Eng Syst Geohazards 13(2):101–130. https://doi.org/10.1080/17499518.2019.1585545

3. Sabatakakis N, Tsiambaos G, Ktena S, Bouboukas S (2018) The effect of microstructure on mi strength parameter variation of common rock types. Bull Eng Geol Environ 77(4):1673–1688. https://doi.org/10.1007/s10064-017-1059-7

4. El Kahi E, Deck O, Khouri M, Mehdizadeh R, Rahme P (2020) A new simplified meta-model to evaluate the transmission of ground movements to structures integrating the elastoplastic soil behavior. Structures 23:324–334. https://doi.org/10.1016/j.istruc.2019.10.023

5. Acharyya R (2019) Finite element investigation and ANN-based prediction of the bearing capacity of strip footings resting on sloping ground. Int J Geo Eng. https://doi.org/10.1186/s40703-019-0100-z

6. Abbas BJ, Aziz HY, Maula BH, Alkateeb RT (2019) Finite element analysis of spread footing near slops. In: IOP conference series materials science and engineering, vol 518, no 2. https://doi.org/10.1088/1757-899x/518/2/022055

7. Munirwan RP, Munirwansyah M (2019) Escape hill as geotechnical quick response method in facing upcoming tsunami disaster. In: IOP conference series earth environmental science, vol 273, no 1. https://doi.org/10.1088/1755-1315/273/1/012053

8. Naseer S, Sarfraz Faiz M, Iqbal S, Jamil SM (2019) Laboratory and numerical based analysis of floating sand columns in clayey soil. Int J Geo Eng 10(1):1–16. https://doi.org/10.1186/s40703-019-0106-6

9. Meng F, Chen R, Kang X, Li Z (2020) e-p curve-based structural parameter for assessing clayey soil structure disturbance. Bull Eng Geol Environ. https://doi.org/10.1007/s10064-020-01833-8

10. Capraru C, Adam D, Hoffmann J, Pelzl M (2014) Numerical analysis of deep excavations and prediction of their influence on neighboring buildings. Numer Methods Geotech Eng 1:1. https://doi.org/10.1201/b17017-132

11. Likitlersuang S, Surarak C, Balasubramania A, Oh E, Ryull KS, Wanatowski D (2013) Duncan-Chang—parameters for hyperbolic stress strain behaviour of soft Bangkok clay. In: 18th international conference on soil mechanics and geotechnical engineering, Paris, pp 381–384. https://doi.org/10.13140/2.1.3744.8966

12. Schanz T, Vermeer PA, Bonnier PG (1999) The hardening soil model: formulation and verification. In: Beyond 2000 in computational geotechnics. Ten years of PLAXIS International. Proceedings of the international symposium, pp 281–296

13. Duncan JM, Chang CY (1970) Nonlinear analysis of stress and strain in soils. J Soil Mech Found Div 96(SM5):1629–1653

14. Herold A, von Wolffersdorff P-A (2009) The use of hardening soil model with small-strain stiffness for serviceability limit state analyses of GRE structures. GeoAfrica 2009:1–8

15. Brinkgreve R (ed) (1999) Beyond 2000 in computational geotechnics. Routledge, London

16. Wu JTH, Tung SC-Y (2020) Determination of model parameters for the hardening soil model. Transp Infrastruct Geotechnol 7(1):55–68. https://doi.org/10.1007/s40515-019-00085-8

17. Honkanadavar NP, Sharma KG (2016) Modeling the triaxial behavior of riverbed and blasted quarried rockfill materials using hardening soil model. J Rock Mech Geotech Eng 8(3):350–365. https://doi.org/10.1016/j.jrmge.2015.09.007

18. Calvello M, Finno RJ (2004) Selecting parameters to optimize in model calibration by inverse analysis. Comput Geotech 31(5):410–424. https://doi.org/10.1016/j.compgeo.2004.03.004

19. Law KH, Othman SZ, Hashim R, Ismail Z (2014) Determination of soil stiffness parameters at a deep excavation construction site in Kenny Hill Formation. Measurement 47(1):645–650. https://doi.org/10.1016/j.measurement.2013.09.030

20. Surarak C, Likitlersuang S, Wanatowski D, Balasubramaniam A, Oh E, Guan H (2012) Stiffness and strength parameters for hardening soil model of soft and stiff Bangkok clays. Soils Found 52(4):682–697. https://doi.org/10.1016/j.sandf.2012.07.009

21. Fu Y, He S, Zhang S, Yang Y (2020) Parameter analysis on hardening soil model of soft soil for foundation pits based on shear rates in Shenzhen Bay, China. Adv Mater Sci Eng 2020:1–11. https://doi.org/10.1155/2020/7810918

22. Saleh S, Mohd Yunus NZ, Ahmad K, Ali N (2018) Stabilization of marine clay soil using polyurethane. In: MATEC Web conference, vol 250, p 01004. https://doi.org/10.1051/matecconf/201825001004

23. BS:1377–8 (1990) Shear strength tests (effective stress). Br. Stand. Inst., London, pp 1–21

24. Paul A, Hussain M (2020) An experiential investigation on the compressibility behavior of cement-treated Indian peat. Bull Eng Geol Environ 79(3):1471–1485. https://doi.org/10.1007/s10064-019-01623-x

25. Head KH (1998) Manual of soil laboratory testing, vol 3, 2nd edn. Wiley, Hoboken, p 215

26. Elkady TY, Abbas MF, Shamrani MA (2016) Behavior of compacted expansive soil under multi-directional stress and deformation boundary conditions. Bull Eng Geol Environ 75(4):1741–1759. https://doi.org/10.1007/s10064-015-0839-1

27. BS:1377-5 (1990) Compressibility, permeability and durability tests. Br. Stand. Inst., London, pp 1–19

28. Hemalatha MS, Santhanam M (2018) Characterizing supplementary cementing materials in blended mortars. Constr Build Mater 191:440–459. https://doi.org/10.1016/j.conbuildmat.2018.09.208

29. Hu W, Nie Q, Huang B, Shu X, He Q (2018) Mechanical and microstructural characterization of geopolymers derived from red mud and fly ashes. J Clean Prod 186:799–806. https://doi.org/10.1016/j.jclepro.2018.03.086

30. Cheng Q, Yao K, Liu Y (2018) Stress-dependent behavior of marine clay admixed with fly-ash-blended cement. Int J Pavement Res Technol 11(6):611–616. https://doi.org/10.1016/j.ijprt.2018.01.004

31. Idinger G, Wu W (2019) Recent advances in geotechnical research. Springer International Publishing, Cham

32. Obrzud RF, Truty A (2018) The hardening soil model—a practical guidebook

33. PLAXIS-3D (2017) Plaxis 3D reference manual

34. Wang F, Han J, Corey R, Parsons RL, Sun X (2017) Numerical modeling of installation of steel-reinforced high-density polyethylene pipes in soil. J Geotech Geoenviron Eng 143(11):04017084. https://doi.org/10.1061/(ASCE)GT.1943-5606.0001784

35. Saleh S, Mohd Yunus NZ, Ahmad K, Ali N, Marto A (2020) Micro-level analysis of marine clay stabilised with polyurethane. KSCE J Civ Eng 24(3):807–815. https://doi.org/10.1007/s12205-020-1797-0

36. Saleh S, Ahmad K, Mohd Yunus NZ, Hezmi MA (2020) Evaluating the toxicity of polyurethane during marine clay stabilisation. Environ Sci Pollut Res 27(17):21252–21259. https://doi.org/10.1007/s11356-020-08549-y

37. Saleh S et al (2019) Geochemistry characterisation of marine clay. In: IOP conference series materials science and

engineering, vol 527, p 012023. https://doi.org/10.1088/1757-899X/527/1/012023

38. Dehghanbanadaki A (2014) Bearing capacity of peat treated with deep mixing cement columns. Universiti Teknologi Malaysia, Johor

39. Ismail Ibrahim KMH (2015) Effect of percentage of low plastic fines on the unsaturated shear strength of compacted gravel soil. Ain Shams Eng J 6(2):413–419. https://doi.org/10.1016/j.asej.2014.10.012

40. Ouhadi VR, Yong RN, Amiri M, Ouhadi MH (2014) Pozzolanic consolidation of stabilized soft clays. Appl Clay Sci 95:111–118. https://doi.org/10.1016/j.clay.2014.03.020

41. Rahman ZA, Yaacob WZW, Rahim SA, Lihan T, Idris WMR, Mohd Sani WNF (2013) Geotechnical characterisation of marine clay as potential liner material. Sains Malays 42(8):1081–1089

42. Nian T, Jiao H, Fan N, Guo X (2020) Microstructure analysis on the dynamic behavior of marine clay in the South China Sea. Mar Georesour Geotechnol 38(3):349–362. https://doi.org/10.1080/1064119X.2019.1573864

43. Jamsawang P, Phongphinittana E, Voottipruex P, Bergado DT, Jongpradist P (2019) Comparative performances of two- and three-dimensional analyses of soil-cement mixing columns under an embankment load. Mar Georesour Geotechnol 37(7):852–869. https://doi.org/10.1080/1064119X.2018.1504261

44. Pakir FB (2017) Physicochemical, microstructural and engineering behaviour of non-traditional stabiliser treated marine clay. Universiti Teknologi Malaysia, Johor

45. Sunny T, Joy A (2016) Study on the effects of marine clay stabilized with banana fibre. Int J Sci Eng Res 4(3):96–98

46. Xiong Y, Liu G, Zheng R, Bao X (2018) Study on dynamic undrained mechanical behavior of saturated soft clay considering temperature effect. Soil Dyn Earthq Eng 115(2017):673–684. https://doi.org/10.1016/j.soildyn.2018.09.026

47. Bo MW, Arulrajah A, Sukmak P, Horpibulsuk S (2015) Mineralogy and geotechnical properties of Singapore marine clay at Changi. Soils Found 55(3):600–613. https://doi.org/10.1016/j.sandf.2015.04.011

48. Bo MW, Choa V, Chu J, Arulrajah A, Horpibulsuk S (2017) Laboratory investigation on the compressibility of Singapore marine clays. Mar Georesour Geotechnol 35(6):847–856. https://doi.org/10.1080/1064119X.2016.1256922

49. Phanvisavakarn P (2018) Strain rate and thermal effect on stress-strain behavior of organic clay. Int J Geomater 15(47):193–200. https://doi.org/10.21660/2018.47.GTE164

50. Ali F, Al-Samaraee EAS (2013) Field behavior and numerical simulation of coastal bund on soft marine clay loaded to failure. Electron J Geotech Eng 18S:4027–4042

51. Otoko GR, Simon AI (2015) Stabilization of a deltaic marine clay (Chikoko) with Chloride compounds. Int Res J Eng Technol 02(03):2095–2097

52. Mesri G, Ajlouni M (2007) Engineering properties of fibrous peats. J Geotech Geoenviron Eng 133(7):850–866. https://doi.org/10.1061/(ASCE)1090-0241(2007)133:7(850)

53. Wang J, Guo L, Cai Y, Xu C, Gu C (2013) Strain and pore pressure development on soft marine clay in triaxial tests with a large number of cycles. Ocean Eng 74:125–132. https://doi.org/10.1016/j.oceaneng.2013.10.005

54. Gu C, Wang J, Cai Y, Sun L, Wang P, Dong Q (2016) Deformation characteristics of overconsolidated clay sheared under constant and variable confining pressure. Soils Found 56(3):427–439. https://doi.org/10.1016/j.sandf.2016.04.009

55. Pakbaz MS, Alipour R (2012) Influence of cement addition on the geotechnical properties of an Iranian clay. Appl Clay Sci 67–68:1–4. https://doi.org/10.1016/j.clay.2012.07.006

56. Saleh S et al (2019) Improving the strength of weak soil using polyurethane grouts: a review. Constr Build Mater 202:738–752. https://doi.org/10.1016/j.conbuildmat.2019.01.048

57. Mohammed Al-Bared MA, Marto A (2017) A review on the geotechnical and engineering characteristics of marine clay and the modern methods of improvements. Malays J Fundam Appl Sci 13(4):825–831. https://doi.org/10.11113/mjfas.v13n4.921

58. Ouahab MY, Mabrouki A, Frank R, Mellas M, Benmeddour D (2020) Undrained bearing capacity of strip footings under inclined load on non-homogeneous clay underlain by a rough rigid base. Geotech Geol Eng 38(2):1733–1745. https://doi.org/10.1007/s10706-019-01127-1

59. Abu El-Soud S, Belal AM (2019) Numerical modeling of rigid strip shallow foundations overlaying geosythetics-reinforced loose fine sand deposits. Arab J Geosci 12(7):254. https://doi.org/10.1007/s12517-019-4436-7

60. Zukri A (2019) Soft clay stabilisation using lightweight aggregate for raft and column matrices. Universiti Teknologi Malaysia

61. Skels P, Bondars K (2017) Applicability of small strain stiffness parameters for pile settlement calculation. Procedia Eng 172:999–1006. https://doi.org/10.1016/j.proeng.2017.02.149

62. Zukri A, Nazir R, Shien NK (2018) Settlement prediction of a group of lightweight aggregate (LECA) columns using finite element modelling. Int J Eng Technol 7(4.35):59. https://doi.org/10.14419/ijet.v7i4.35.22324

63. Samadhiya NK (2017) Numerical analysis of anchored granular pile (AGP) under tensile loads. In: 19th international conference on soil mechanics and geotechnical engineering, Seoul, pp 3231–3234

64. Momeni E, Maizir H, Gofar N, Nazir R (2013) Comparative study on prediction of axial bearing capacity of driven piles in granular materials. J Teknol (Sciences Eng) 61(3):15–20. https://doi.org/10.11113/jt.v61.1777

65. Zheng A (2018) Finite element analysis on bearing capacity of post-grouting bored pile with the HS-small model and the HS model. IOP Conf Ser Earth Environ Sci 189(2). https://doi.org/10.1088/1755-1315/189/2/022087